




RESEARCH ARTICLE | MARCH 08 2024

Accurate evaluation method for HRS retention of VCM ReRAM

N. Kopperberg ; D. J. Wouters ; R. Waser ; S. Menzel ; S. Wiefels  

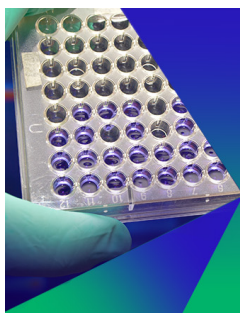


APL Mater. 12, 031112 (2024)

<https://doi.org/10.1063/5.0188573>



CrossMark



Biomicrofluidics

Special Topic:
Microfluidics and Nanofluidics in **India**

Submit Today



Accurate evaluation method for HRS retention of VCM ReRAM

Cite as: APL Mater. 12, 031112 (2024); doi: 10.1063/5.0188573

Submitted: 22 November 2023 • Accepted: 7 February 2024 •

Published Online: 8 March 2024



N. Kopperberg,¹ D. J. Wouters,¹ R. Waser,^{1,2,3} S. Menzel,² and S. Wiefels^{2,a)}

AFFILIATIONS

¹ Institut für Werkstoffe der Elektrotechnik II (IWE2) and JARA-FIT, RWTH Aachen University, 52074 Aachen, Germany

² Peter-Grünberg-Institut 7 (PGI-7), Forschungszentrum Jülich GmbH, 52425 Jülich, Germany

³ Peter-Grünberg-Institut 10 (PGI-10), Forschungszentrum Jülich GmbH, 52425 Jülich, Germany

^{a)} Author to whom correspondence should be addressed: s.wiefels@fz-juelich.de

ABSTRACT

Long-term retention is one of the major challenges concerning the reliability of redox-based resistive switching random access memories based on the valence change mechanism (VCM). The stability of the programmed state has to be ensured over several years, leaving a sufficient read window between the states, which is even more challenging at large statistics. Thus, the underlying physical mechanisms have to be understood and experimental data have to be evaluated accurately. Here, it shows that the retention behavior of the high resistive state (HRS) is more complex than that of the low resistive state and requires a different evaluation method. In this work, we experimentally investigate the retention behavior of 5M VCM devices via accelerated life testing and show the difficulties of commonly used evaluation methods in view of the HRS. Subsequently, we present a new evaluation method focusing on the standard deviation of the HRS current distribution. Hereby, an activation energy for the degradation process can be extracted, which is essential for the prediction of the devices' behavior under operating conditions. Furthermore, we reproduce the experimentally observed behavior with our 3D Kinetic Monte Carlo simulation model. We confirm the plausibility of our evaluation method and are able to connect the calculated activation energy to the migration barriers of oxygen vacancies that we implemented in the model and that we believe play a key role in the experimentally observed degradation process.

© 2024 Author(s). All article content, except where otherwise noted, is licensed under a Creative Commons Attribution (CC BY) license (<http://creativecommons.org/licenses/by/4.0/>). <https://doi.org/10.1063/5.0188573>

I. INTRODUCTION

Regarding the increasing demand of non-volatile memories (NVMs) due to the advancing digitization of numerous areas of our everyday life, the research in the field of new technologies was strongly expanded over the last years.^{1,2} Here, redox-based resistive switching random access memory (ReRAM) seems to be a promising candidate to replace the typically used flash technology, which is expected to reach its physical limits soon.^{3–5} Numerous publications have shown the advantages of ReRAM, e.g., fast switching speed down to 20 ps,^{6,7} high scalability with sub-10 nm² cells,^{8,9} and low operating voltages (<2 V).^{10,11} Additionally, ReRAM could be a key component in neuromorphic computing applications.¹²

Thus, bipolar switching valence change mechanism (VCM) based ReRAM cells are extensively studied. Typically, they consist of a transition metal–oxide layer placed between two metal electrodes with a high work function (electrochemically active electrode,

AE) and a low work function (ohmic electrode, OE).^{13,14} By applying external voltages, oxygen vacancies ($V_{\text{O}}^{\bullet\bullet}$) as one type of mobile donors can be generated in a so-called forming step, building a conductive filament through the oxide layer.^{15,16} Afterward, the filament can be ruptured by moving $V_{\text{O}}^{\bullet\bullet}$ away from the AE, leaving behind a depletion zone, also called gap, and consecutively rebuilt depending on the voltage polarity. Hereby, the cell can be switched between a high resistive state (HRS) and a low resistive state (LRS), which can be read out non-destructively by applying a comparatively small read voltage.^{13,17}

Since VCM ReRAM devices are currently crossing the line to commercial breakthrough, reliability aspects get more and more into the focus.^{18,19} Here, a typical requirement for NVM applications of ReRAM is a long-time stability of the programmed states, called retention, for 5–10 years at an operating temperature of 85–125 °C.²⁰ For applications in an automotive environment, even operating temperatures up to 175 °C have to be considered.¹⁸ In

order to investigate the retention behavior, accelerated life testing (ALT), where the cells are exposed to elevated temperatures, plays an important role. In this context, it is customary to determine the activation energy E_A of the underlying temperature-activated process in order to make predictions for the retention behavior on acceptable timescales.^{21–23} The exact process is still unclear but can in our opinion only be related to the diffusion, generation, and recombination of V_O^\bullet . Often, the exact process is not examined at all, but E_A is simply determined from the electrical signal.

So far, in literature, the focus of retention investigations concerning VCMs mostly lies on the LRS in experimental works^{22–25} as well as via simulations.^{26–29} As the LRS current distribution is typically observed to mainly shift at elevated temperatures, its behavior can be extrapolated comparatively easy. Nevertheless, the HRS retention has been presented in several experimental works.^{30–32} However, so far, only the mean value or single devices have been considered for the HRS retention characterization. With regard to the different retention behavior of the investigated cells (decreasing or increasing current), this contemplation is in our opinion deficient. In the few available studies of the HRS retention via simulation models,^{29,33–35} the mean current is usually in the focus as well, variability is not adequately considered, and to our knowledge no activation energy E_A has been calculated from the simulated HRS retention data and connected to the physical model behind. Ultimately, the retention of both HRS and LRS has to be understood because the key challenge is a sufficient read window between these two states after the required storage time at operating temperature.

Thus, in this work, we investigate the retention behavior of the HRS. We present experimental data that reveal the more complicated behavior of the HRS, looking at cell statistics. We show that the typical LRS evaluation methods cannot be adopted for the HRS and hence introduce a new evaluation method for the HRS retention. We found that considering the statistics (e.g., the current distribution) of many devices and especially looking at the standard deviation are more successful than looking at single cells or mean currents.

Furthermore, we support our experimental findings and the introduced evaluation method via our 3D Kinetic Monte Carlo (KMC) model, which was initially presented in Ref. 36. With our simulation model, we show similar HRS retention behavior that is based on the random diffusion of V_O^\bullet . Finally, we prove that with our evaluation method, an activation barrier can be extracted that coincides with the diffusion energy barrier implemented in our model for long-range diffusion.

II. EXPERIMENTAL

A. Details

The experimental study is based on a 28 nm back end of line (BEOL) integrated VCM type ReRAM from a collaboration with Infineon Technologies. Information that is more detailed can be found in Ref. 37. On five equal dies, 5.6M devices each are prepared by electroforming and pre-cycling. Each programming operation is performed via a program-verify algorithm consisting of several steps in order to program HRS and LRS into defined resistance ranges. After preparation, one half of the devices (2.8 Mbit) on each die is programmed into HRS and the second half into LRS. Subsequently, all devices are read by applying a pulse of 0.2 V. In order to estimate

the room temperature retention on long time scales, ALT is applied. Thus, each die is baked at a different temperature, ranging from 125 to 250 °C, and in between read again at room temperature. This provides the degradation over time and temperature from which the correct trend needs to be extracted for a reliable estimation of the long term retention. It might be noted that the measurement is conducted on a test vehicle. Thus, chip and algorithm deviate from the optimized product versions.³⁸

B. Results

The resulting distributions for one exemplary die after programming are depicted by blue lines in Fig. 1. The distributions are given in a quantile plot, i.e., they are normalized with the standard normal distribution. Thus, the ordinate is given in multiples of the standard deviation σ . After bake at 150 °C for up to 30 h, the LRS only shows a minor shift toward lower read current. In order to extrapolate its degradation, the Arrhenius approach is a common method, which proved to be valid.^{21–23} In the LRS, the degradation can be directly measured using simply the current change ΔI after a specific bake-time compared to the state directly after programming I_0 .

However, the degradation of the HRS shows a complex behavior as it is comprised of a shift to lower currents as well as a broadening over time. As an example of a suboptimal approach, the Arrhenius method is applied using simply ΔI in Fig. 2. First, the change in read current for different bake temperatures is evaluated at different quantiles (σ) of the HRS distributions and plotted over $\log(t)$ in Fig. 2(a). In order to reliably apply the Arrhenius model, the degradation over $\log(t)$ should follow a straight line while being parallel to the degradation at different temperatures. By chance, the data for -4σ seem to nearly fulfill this criterion. However, the individual slopes strongly depend on the quantile of evaluation. Starting from -2σ , even a negative degradation is observed. At 0σ (i.e., the median), some extracted values strongly deviate toward high negative values, as indicated by the dashed fit. As demonstrated in Fig. 2(b), no reliable Arrhenius plot can be generated from these data. Evaluating ΔI at -1σ or 0σ completely breaks the Arrhenius model, as indicated by the dashed fits.

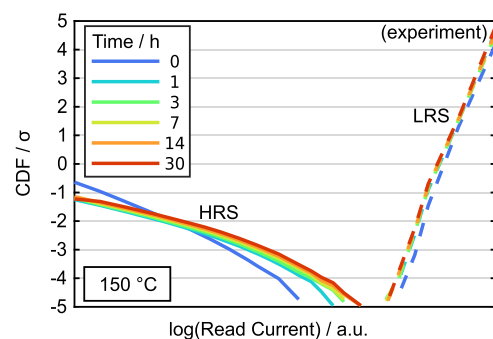


FIG. 1. Normalized cumulative distributions of exemplary retention results. 2.8M devices are programmed into HRS (solid lines) and LRS (dashed lines) each. Subsequently, the die is baked at 150 °C for up to 30 h as specified in the legend. The LRS only shows a slide shift toward lower read current. The HRS shows a complex degradation comprising shifting and tilting.

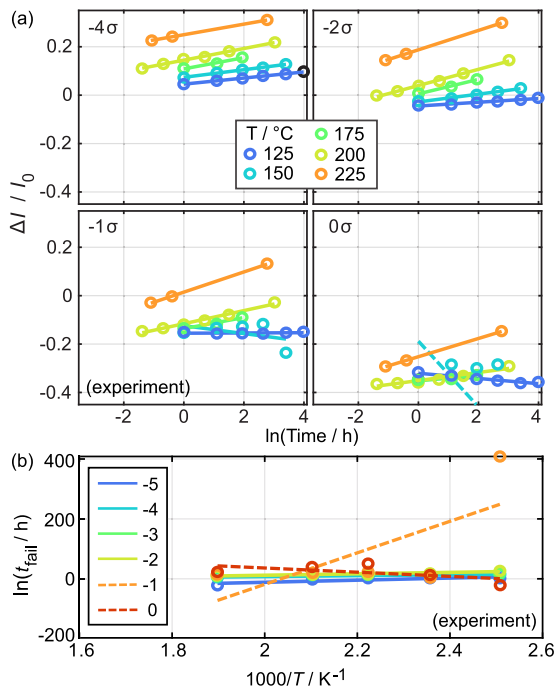


FIG. 2. Suboptimal approach to determine E_A : (a) Degradation of the read current evaluated from different quantiles (σ) of the distribution, revealing strong dependency on where ΔI is evaluated. (b) Arrhenius plot of the degradation for different quantiles (σ). No clear E_A can be determined. For -1σ and 0σ that correspond to the median, the Arrhenius model completely breaks (dashed lines).

Thus, a more reliable approach to determine an activation energy E_A for degradation is required. We propose to utilize the statistical parameters of the HRS data and extrapolate their trend over t . Accordingly, the HRS read current distributions are fitted

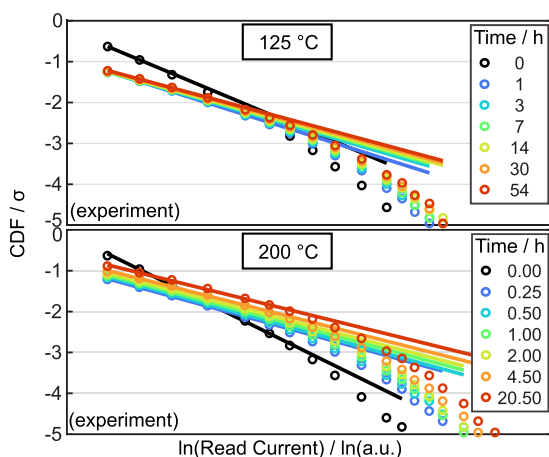


FIG. 3. Linear fit of the log-normal HRS distribution demonstrated exemplarily on the degradation at 125 and 200 °C. The distributions monotonously tilt toward higher standard deviation σ [regarding $\log(I)$].

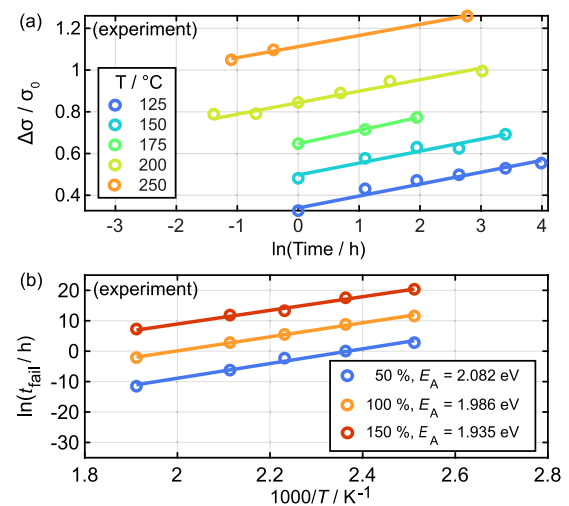


FIG. 4. (a) The normalized degradation of the standard deviation $\Delta\sigma / \sigma_0$ [regarding $\log(I)$] is extracted from the fits in Fig. 3 and plotted over $\log(t)$. The resulting parallel lines indicate the validity of the Arrhenius approach. (b) Extracted failure time for different levels of σ degradation added to an Arrhenius plot, resulting in excellent fits and an extracted E_A around 2 eV.

as shown exemplarily using the 125 and 200 °C degradation data in Fig. 3.

Here, the plotting of normal quantiles over $\log(t)$ allows for applying a linear fit to match the log-normal statistics.³⁹ Note that a large part to the left of the distribution is cut off. Here, the sense amplifier sweep only detects that the read current is smaller than the lowest reference current and thus not critical for the read window. Nevertheless, previous studies showed that the log-normal trend as fitted here continues for the major part of the distribution and only the right tail deviates from the log-normal statistics.^{39,40}

From these fits, the characteristic parameters μ and σ of the log-normal distribution are extracted. Here, μ is the median and σ is the standard deviation of $\log(I)$. The plots in Fig. 3 emphasize that the tilting or broadening of the distributions has the highest impact on the right edge of the distribution and that on the read window. Thus, it is reasonable to focus on the increase in σ , which corresponds to the reciprocal slope of the fit. Figure 4(a) shows the relative increase in σ over the bake time for all five bake temperatures.

These trends are fitted linearly over $\log(t)$. In contrast to Fig. 2(a), the slopes of these fits are very consistent and already show a spacing proportional to the temperature. Accordingly, Fig. 4(b) provides exceptional Arrhenius fits over a broad range of changes in σ . Here, an increase of σ in the range from 50 % to 150 % compared to the initial distribution after programming is taken into account. These fits result in extracted E_A around 2 eV as specified in the legend. This can be considered a reasonable value for the migration of $V_O^{\bullet\bullet}$ in typical VCM type ReRAM materials.^{41,42}

In total, this evaluation method is easy to use and seems to provide very reliable results. However, this is not sufficient as a proof of validity and it needs to be confirmed that the extracted E_A corresponds to an underlying physical process.

III. SIMULATION

In order to confirm the experimental findings and to validate the proposed evaluation method, as well as to build a connection between the extracted activation energy E_A and its physical origin, we used our 3D KMC simulation model, first introduced in Ref. 36. The simulation model consists of a cubic lattice structure with a spacing of 0.5 nm between each lattice point, representing a $(6 \text{ nm})^3$ HfO_x layer sandwiched between two metal electrodes. Depending on the externally applied voltage and the distribution of the $V_O^{\bullet\bullet}$ at the lattice points, the potential can be calculated via solving Poisson's equation. The current through the cell is determined by the usage of a trap-assisted tunneling (TAT) solver. The TAT conduction mechanism accurately describes the behavior of systems with comparatively low $V_O^{\bullet\bullet}$ concentrations, as it is the case for the HRS that we investigate in our study.⁴³

The fundamental component of the simulation model is the KMC process, which allows for incorporating random processes and consequently precisely portraying the statistics of the devices. As demonstrated in our previous work, the diffusion of $V_O^{\bullet\bullet}$ is of major importance concerning the reliability of VCM ReRAM.^{36,37} In our model, the drift/diffusion rates are calculated for all $V_O^{\bullet\bullet}$ and for all possible directions via

$$R_D = v_0 \exp\left(-\frac{E_D - e\Delta\Phi}{k_B T}\right), \quad (1)$$

where $v_0 = 10^{12}$ Hz denotes the characteristic vibration frequency, E_D denotes the drift/diffusion energy barrier, and $\Delta\Phi$ denotes the potential barrier between the two positions. Subsequently, one process is chosen randomly but weighted by the rates and executed followed by a time update. In Ref. 36, diffusion-limiting domains were introduced as small boxes with a typical diffusion barrier of $E_D = 0.7$ eV inside and a hindered diffusion barrier of $E_D' = 1.2$ eV from box to box. Thus, we were able to explain and reproduce several short-term instability and long-term retention phenomena consistently in the same model by the same physical origin, namely, the $V_O^{\bullet\bullet}$ diffusion. More details of the model can be found in Ref. 36.

A. Results

In accordance with the experiments presented before, ALT simulations, also called baking simulations, were conducted. Thus, 100 cells were programmed into the HRS by randomly placing 60 $V_O^{\bullet\bullet}$ in a $2 \times 2 \times 3 \text{ nm}^3$ filament with a 3 nm gap to the AE, respectively. In the dark blue curve in Fig. 5, the initial current distribution for an applied read voltage of 0.3 V can be seen. The linear behavior of the current distribution in the plot with a logarithmic x axis shows the log-normal behavior that is typically observed for the HRS. Now, the cells are exposed to elevated temperatures. In total, six different temperatures were investigated with 100 cells, each comprising the properties mentioned above. The temperatures in the simulations were set in a range from 950 to 1400 K, which is significantly higher compared to the experiments. This range was chosen to avoid the high computational effort, which is inherent in these types of simulations if the temperatures are relatively low. Choosing high temperatures leads to very short baking times in the nano- to microsecond range and consequently to shorter computation times.

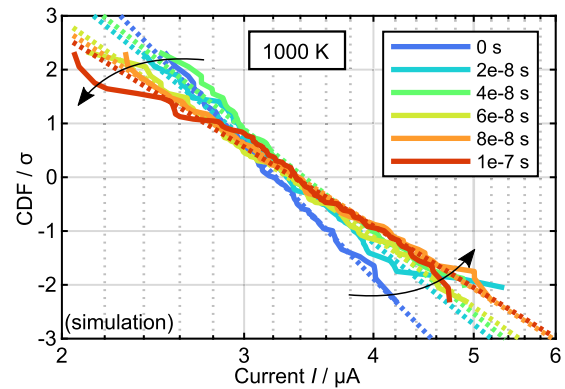


FIG. 5. Current distribution of 100 cells programmed to the HRS during simulated baking at 1000 K. As implied by the black arrows, the current distribution tilts over time, whereas the mean current stays nearly constant. The dotted lines are linearly fitted to the data with respect to the typical log-normal behavior of the HRS current distribution.

In Fig. 5, the time evolution of the current distribution is shown for a bake at 1000 K. It should be mentioned that the current is calculated for every time step, without actually applying the read voltage. Thus, as in the experiments, the cells do not see a voltage during the baking. As the arrows in Fig. 5 indicate, the current distribution tilts over time, finally leading to a wider distribution (red) with higher and lower resistive cells than before the bake. This tilt can be attributed to the combination of the radial and the vertical diffusion into the gap of $V_O^{\bullet\bullet}$ as presented in our previous work in Ref. 36. Cells with predominating radial $V_O^{\bullet\bullet}$ diffusion and thus decreasingly dense filament have a lowered read current, whereas the cells with predominating $V_O^{\bullet\bullet}$ jumps into the gap and decreased tunnel barrier have an increased current. Consequently, the distribution broadens, whereas the mean value of the current distribution remains almost constant over time. As demonstrated in our previous work, a shift of the distribution to higher or lower currents could also be observed depending on the initial conditions,³⁶ but is typically less important than the effect of the tilt.³⁹

In order to investigate the retention behavior quantitatively, a linear fit has been applied to the current distributions for all times during baking. From the slopes of the linear fits, the standard deviation of the log-normal distributions can be extracted. The time evolution of the normalized standard deviation of the current distributions is represented in Fig. 6 for all six simulated baking temperatures. After a comparatively short, noisy starting phase, the standard deviations for all simulated temperatures increase up to at most 130% in the simulated time-range. The increase shows several fluctuations that can be attributed to the high influence of single random events on the current distribution of merely 100 simulated cells each. Despite the noisy behavior, the increase of the standard deviation overall follows a linear trend. In Fig. 6, the standard deviation has been fitted linearly, neglecting the noisy start phase that is marked by the gray box at the bottom. It can be seen that the linear fits have a very similar slope for all temperatures and are only shifted horizontally to each other.

As motivated before, the increase of the standard deviation can be used as a reasonable failure criterion for the retention of VCMs.

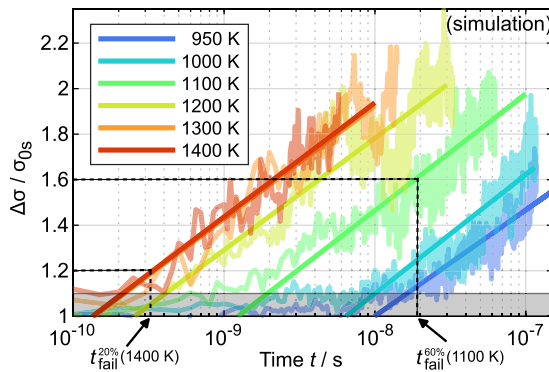


FIG. 6. Normalized standard deviation of the current distributions of each 100 cells for ALT simulations with six different temperatures over time. After a short, noisy start phase (gray box), the standard deviations increase overall linearly, as depicted by the linear fits for each temperature. The extraction of failure times is exemplarily shown for two different limits and two different temperatures (black dashed lines).

Furthermore, E_A of the underlying process can be extracted from the data, which is necessary to make predictions for the retention of VCMs at normal operation temperatures. Thus, the failure criterion has to be chosen reasonably. On the one hand, the failure limit should be higher than the general noise of the standard deviation. On the other hand, the failure limit is confined by the simulated data of the curve with the highest temperature. Hence, failure limits in a range from a 20%–60% increase in the standard deviation with a step size of 1% were used for our simulated data. The corresponding failure times t_{fail} are extracted for the raw simulated data, as well as for the linear fits in Fig. 6. Subsequently, the failure times are presented in a typical Arrhenius plot in Fig. 7. The failure times extracted from the raw data are shown in Fig. 7(a), and the failure times of the fitted data can be seen in Fig. 7(b).

Now, via the slope of the linear fits in Fig. 7, activation energies E_A can be calculated for both variants and each failure criterion following Arrhenius' law. The calculated E_A are shown in Fig. 8 for both variants, the raw (blue) and the fitted (red) data, as well as the

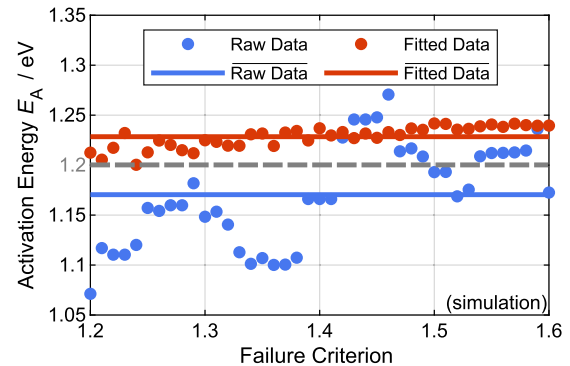


FIG. 8. Calculated E_A depending on the failure criterion for the two methods with the raw data (blue dots) and the fitted data (red dots). The horizontal lines indicate the mean values. The gray dashed line depicts the expected value of 1.2 eV that was implemented in the model. The raw data are comparatively noisy, although both mean values are equally close to the expected value.

corresponding mean values. Whereas the activation energies from the fitted data are nearly constant, it can be observed that the activation energies from the raw data are strongly dependent on the respective failure criterion. Nevertheless, the mean values of both variants are with a deviation of less than 2.5% very close to the expected value of 1.2 eV (gray dashed line) of the hindered box-to-box diffusion that is crucial for the retention behavior, following our previous studies.^{36,37} The comparison with the experimentally calculated value (~ 2.0 eV) reveals that the implemented value of E_D' in the simulation should be adjusted to higher values for future works.

These findings indicate that with our evaluation method, it is actually possible to extract physical information of the diffusion processes, which are responsible for the retention failure of VCM ReRAM devices. Furthermore, in contrast to looking at mean values or the tails of the distribution, it is possible to extract an activation energy with our method for the retention behavior of the HRS. The opportunity of extracting an activation energy in ALT is indispensable to make predictions for retentions of the cells over long times under normal operation conditions.

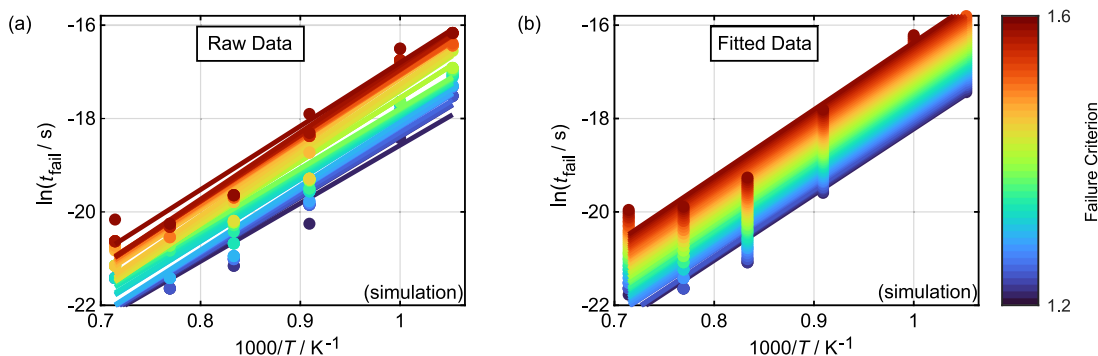


FIG. 7. Arrhenius plot for the different failure criteria. In (a), the failure times were extracted for the raw data from Fig. 6, whereas in (b), the fitted data were consulted. Linear fits have been applied to all failure criteria to extract the underlying activation energies E_A .

IV. CONCLUSIONS

In this study, we presented the retention behavior of a 5.6M 28 nm BEOL integrated VCM type ReRAM by conducting ALT. Whereas the LRS is comparatively stable and can be easily evaluated by the shift of the mean value of the current distribution, the HRS shows a more complex behavior. We showed that the simple contemplation of the current shift is not sufficient to apply the Arrhenius model and to extract an activation energy. Consequently, a more appropriate evaluation method was introduced, which focuses on the evolution of the standard deviation of the current distribution during baking. Thereby, we were able to accurately calculate an activation energy for the retention degradation of the devices, which fits to the migration barrier of $V_O^{\bullet\bullet}$ in typically used oxides.

Additionally, ALT simulations via a 3D KMC model were conducted, which nicely reproduce the experimentally observed tilt of the HRS current distributions. Again, the time evolution of the standard deviation was extracted and the activation energy of the underlying process was calculated. This was done from the original data as well as from the fitted increase of the standard deviation. Both methods lead to a similar result, looking at the mean value, while the activation energy extracted from the fitted data is nearly independent of the predefined failure criterion. Finally, we found that the extracted activation energy is nearly identical with the migration barrier of $V_O^{\bullet\bullet}$ implemented in the simulation model and thus affirms our idea of the physical origin of the degradation process concerning VCM ReRAM retention.

ACKNOWLEDGMENTS

This work was supported by the Federal Ministry of Education and Research (BMBF, Germany) in the project NEU-ROTEC (Project Nos. 16ME0398K and 16ME0399). It is based on the Jülich Aachen Research Alliance (JARA-FIT). The authors gratefully acknowledge computing time on the supercomputer JURECA⁴⁴ at Forschungszentrum Jülich under Grant No. 27525. They would also like to show their gratitude to Karl Hofmann and Jan Otterstedt for providing experimental data and fruitful discussions.

AUTHOR DECLARATIONS

Conflict of Interest

The authors have no conflicts to disclose.

Author Contributions

N.K. designed and carried out simulations, analyzed data and wrote the manuscript. D.J.W. validated and reviewed. R.W. supervised. S.M. validated, reviewed and supervised. S.W. conceived the concept, analyzed data and co-wrote the manuscript.

N. Kopperberg: Data curation (equal); Investigation (equal); Writing – original draft (lead). **D. J. Wouters:** Validation (equal).

R. Waser: Supervision (equal). **S. Menzel:** Supervision (equal); Validation (equal). **S. Wiefels:** Conceptualization (lead); Data curation (equal); Investigation (equal); Writing – original draft (supporting).

DATA AVAILABILITY

The data that support the findings of this study are available within the article.

REFERENCES

- Y. Chen, "ReRAM: History, status, and future," *IEEE Trans. Electron Devices* **64**, 1–14 (2020).
- Z. Wang, H. Wu, G. W. Burr, C. S. Hwang, K. L. Wang, Q. Xia, and J. J. Yang, "Resistive switching materials for information processing," *Nat. Rev. Mater.* **5**, 173–195 (2020).
- R. Dittmann, S. Menzel, and R. Waser, "Nanoionic memristive phenomena in metal oxides: The valence change mechanism," *Adv. Phys.* **70**, 155–349 (2021).
- G. W. Burr, R. M. Shelby, A. Sebastian, S. Kim, S. Kim, S. Sidler, K. Virwani, M. Ishii, P. Narayanan, A. Fumarola, L. L. Sanches, I. Boybat, M. Le Gallo, K. Moon, J. Woo, H. Hwang, and Y. Leblebici, "Neuromorphic computing using non-volatile memory," *Adv. Phys.: X* **2**, 89–124 (2017).
- D. V. Christensen *et al.*, "2022 roadmap on neuromorphic computing and engineering," *Neuromorphic Comput. Eng.* **2**, 022501 (2022).
- M. Csontos, Y. Horst, N. J. Olalla, U. Koch, I. Shorubalko, A. Halbritter, and J. Leuthold, "Picosecond time-scale resistive switching monitored in real-time," *Adv. Electron. Mater.* **9**, 2201104 (2023).
- M. von Witzleben, S. Wiefels, A. Kindsmüller, P. Stasner, F. Berg, F. Cüppers, S. Hoffmann-Eifert, R. Waser, S. Menzel, and U. Böttger, "Intrinsic reset speed limit of valence change memories," *ACS Appl. Electron. Mater.* **3**, 5563–5572 (2021).
- Y. Hou, U. Celano, L. Goux, L. Liu, A. Fantini, R. Degraeve, A. Youssef, Z. Xu, Y. Cheng, J. Kang, M. Jurczak, and W. Vandervorst, "Sub-10 nm low current resistive switching behavior in hafnium oxide stack," *Appl. Phys. Lett.* **108**, 123106 (2016).
- U. Celano, A. Fantini, R. Degraeve, M. Jurczak, L. Goux, and W. Vandervorst, "Scalability of valence change memory: From devices to tip-induced filaments," *AIP Adv.* **6**, 085009 (2016).
- B. Govoreanu, G. S. Kar, Y.-Y. Chen, V. Paraschiv, S. Kubicek, A. Fantini, I. P. Radu, L. Goux, S. Clima, R. Degraeve, N. Jossart, O. Richard, T. Vandeweyer, K. Seo, P. Hendrickx, G. Pourtois, H. Bender, L. Altimime, D. J. Wouters, J. A. Kittl, and M. Jurczak, "10 × 10 nm² Hf/HfO_x crossbar resistive ram with excellent performance, reliability and low-energy operation," in *2011 IEEE International Electron Devices Meeting (IEDM) (IEDM Tech. Dig.)* (IEEE, 2011) Vol. 31, pp. 6.1–6.4.
- B. J. Choi, A. C. Torrezan, J. P. Strachan, P. G. Kotula, A. J. Lohn, M. J. Marinella, Z. Li, R. S. Williams, J. J. Yang, and J. J. Yang, "High-speed and low-energy nitride memristors," *Adv. Funct. Mater.* **26**, 5290–5296 (2016).
- D. Ielmini, Z. Wang, and Y. Liu, "Brain-inspired computing via memory device physics," *APL Mater.* **9**, 050702 (2021).
- R. Waser, R. Bruchhaus, and S. Menzel, "Redox-based resistive switching memories," in *Nanoelectronics and Information Technology*, 3rd ed. (Wiley VCH, Hoboken, NJ, 2012), pp. 683–710.
- H.-S. P. Wong, H.-Y. Lee, S. Yu, Y.-S. Chen, Y. Wu, P.-S. Chen, B. Lee, F. T. Chen, and M.-J. Tsai, "Metal-oxide RRAM," *Proc. IEEE* **100**, 1951–1970 (2012).
- J.-Y. Chen, C.-W. Huang, C.-H. Chiu, Y.-T. Huang, and W.-W. Wu, "Switching kinetic of VCM-based memristor: Evolution and positioning of nanofilament," *Adv. Mater.* **27**, 5028–5033 (2015).
- S. Menzel and J.-H. Hur, *Modeling the VCM- and ECM-type Switching Kinetics* (Wiley VCH, 2016), pp. 395–436.
- D. Cooper, C. Baeumer, N. Bernier, A. Marchewka, C. La Torre, R. E. Dunin-Borkowski, S. Menzel, R. Waser, and R. Dittmann, "Anomalous resistance hysteresis in oxide ReRAM: Oxygen evolution and reincorporation revealed by in situ tem," *Adv. Mater.* **29**, 1700212 (2017).

- ¹⁸R. Strenz, "Review and outlook on embedded NVM technologies—From evolution to revolution," in *International Memory Workshop* (IEEE, 2020), pp. 1–4.
- ¹⁹F. Zahoor, F. A. Hussin, U. B. Isyaku, S. Gupta, F. A. Khanday, A. Chattopadhyay, and H. Abbas, "Resistive random access memory: Introduction to device mechanism, materials and application to neuromorphic computing," *Nanoscale Res. Lett.* **18**, 1–49 (2023).
- ²⁰D. J. Wouters, Y.-Y. Chen, A. Fantini, and N. Raghavan, "Reliability aspects," in *Resistive Switching. From Fundamentals of Nanoionic Redox Processes to Memristive Device Applications*, edited by D. I. R. Waser (Wiley, 2016).
- ²¹B. Gao, J. Kang, H. Zhang, B. Sun, B. Chen, L. Liu, X. Liu, R. Han, Y. Wang, Z. Fang, H. Yu, B. Yu, and D.-L. Kwong, "Oxide-based RRAM: Physical based retention projection," in *2010 Proceedings of the European Solid State Device Research Conference* (IEEE, 2010), pp. 392–395.
- ²²E. Perez, M. K. Mahadevaiah, C. Zambelli, P. Olivo, and C. Wenger, "Data retention investigation in Al:HfO₂-based resistive random access memory arrays by using high-temperature accelerated tests," *J. Vac. Sci. Technol., B: Microelectron. Nanometer Struct.–Process., Meas., Phenom.* **37**, 012202 (2019).
- ²³D. Ielmini, F. Nardi, C. Cagli, and A. L. Lacaita, "Size-dependent retention time in NiO-based resistive-switching memories," *IEEE Electron Device Lett.* **31**, 353–355 (2010).
- ²⁴B. Traoré, P. Blaise, E. Vianello, H. Grampeix, S. Jeannot, L. Perniola, B. De Salvo, and Y. Nishi, "On the origin of low-resistance state retention failure in HfO₂-based RRAM and impact of doping/alloying," *IEEE Trans. Electron Devices* **62**, 4029–4036 (2015).
- ²⁵Y.-L. Wang, Y.-L. Song, L.-M. Yang, Y.-Y. Lin, R. Huang, Q.-T. Zou, and J.-G. Wu, "Algorithm-enhanced retention based on megabit array of Cu_xSi_yO RRAM," *IEEE Electron Device Lett.* **33**, 1408–1410 (2012).
- ²⁶S. Aldana, E. Pérez, F. Jiménez-Molinos, C. Wenger, and J. B. Roldán, "Kinetic Monte Carlo analysis of data retention in Al: HfO₂-based resistive random access memories," *Semicond. Sci. Technol.* **35**, 115012 (2020).
- ²⁷N. Raghavan, D. D. Frey, M. Bosman, and K. L. Pey, "Statistics of retention failure in the low resistance state for hafnium oxide RRAM using a kinetic Monte Carlo approach," *Microelectron. Reliab.* **55**, 1422–1426 (2015).
- ²⁸J. T. Jang, G. Ahn, S.-J. Choi, D. M. Kim, H. Kim, and D. H. Kim, "LRS retention fail based on joule heating effect in InGaZno resistive-switching random access memory," *Appl. Phys. Express* **13**, 054004 (2020).
- ²⁹T. Ninomiya, Z. Wei, S. Muraoka, R. Yasuhara, K. Katayama, and T. Takagi, "Conductive filament scaling of TaO_x bipolar rram for improving data retention under low operation current," *IEEE Trans. Electron Devices* **60**, 1384–1389 (2013).
- ³⁰Y. Y. Chen, M. Komura, R. Degraeve, B. Govoreanu, L. Goux, A. Fantini, N. Raghavan, S. Clima, L. Zhang, A. Belmonte, A. Redolfi, G. S. Kar, G. Groeseneken, D. J. Wouters, and M. Jurczak, "Improvement of data retention in HfO₂/Hf 1T1R RRAM cell under low operating current," in *2013 IEEE International Electron Devices Meeting* (IEEE, 2013), pp. 10.1.1–10.1.4.
- ³¹Y.-H. Lin, Y.-H. Ho, M.-H. Lee, C.-H. Wang, Y.-Y. Lin, F.-M. Lee, K.-C. Hsu, P.-H. Tseng, D.-Y. Lee, K.-H. Chiang, K.-C. Wang, T.-Y. Tseng, and C.-Y. Lu, "A comprehensive study of 3-stage high resistance state retention behavior for TMO ReRAMS from single cells to a large array," in *2017 IEEE International Electron Devices Meeting (IEDM)* (IEEE, 2017), pp. 2.5.1–2.5.4.
- ³²J. Frascaroli, F. G. Volpe, S. Brivio, and S. Spiga, "Effect of al doping on the retention behavior of HfO₂ resistive switching memories," *Microelectron. Eng.* **147**, 104–107 (2015), part of special issue Insulating Films on Semiconductors 2015.
- ³³K. Maeda, S. Matsuda, K. Takeuchi, and R. Yasuhara, "Observation and analysis of bit-by-bit cell current variation during data-retention of TaO_x-based rram," in *2018 48th European Solid-State Device Research Conference (ESSDERC)* (IEEE, 2018), pp. 46–49.
- ³⁴Z. Wei, T. Takagi, Y. Kanzawa, Y. Katoh, T. Ninomiya, K. Kawai, S. Muraoka, S. Mitani, K. Katayama, S. Fujii, R. Miyanaga, Y. Kawashima, T. Mikawa, K. Shimakawa, and K. Aono, "Retention model for high-density ReRAM," in *2012 4th IEEE International Memory Workshop* (IEEE, 2012), pp. 1–4.
- ³⁵L. Cai, W. Chen, Y. Zhao, X. Liu, J. Kang, X. Zhang, and P. Huang, "Insight into effects of oxygen reservoir layer and operation schemes on data retention of HfO₂-based RRAM," *IEEE Trans. Electron Devices* **66**, 3822–3827 (2019).
- ³⁶N. Kopperberg, S. Wiefels, S. Liberda, R. Waser, and S. Menzel, "A consistent model for short-term instability and long-term retention in filamentary oxide-based memristive devices," *ACS Appl. Mater. Interfaces* **13**, 58066–58075 (2021).
- ³⁷S. Wiefels, N. Kopperberg, K. Hofmann, J. Otterstedt, D. Wouters, R. Waser, and S. Menzel, "Reliability aspects of 28 nm BEOL-integrated resistive switching random access memory," *Phys. Status Solidi A*, 2300401 (2023).
- ³⁸Infineon Technologies AG, Infineon and TSMC to introduce RRAM technology for automotive AURIX™ TC4x product family (2022); <https://www.infineon.com/cms/en/about-infineon/press/market-news/2022/INFATV202211-031.html>
- ³⁹S. Wiefels, U. Böttger, S. Menzel, D. J. Wouters, and R. Waser, "Statistical modeling and understanding of hrs retention in 2.5 mb HfO₂ based ReRAM," in *2020 IEEE International Memory Workshop (IMW) (2020 IEEE 12th International Memory Workshop)* (IEEE, Dresden, Germany, 2020), pp. 28–31.
- ⁴⁰S. Wiefels, "Reliability aspects in resistively switching valence change memory cells," Ph.D. thesis, Rheinisch-Westfälische Technische Hochschule Aachen, 2021.
- ⁴¹J. Hur, "Theoretical studies on oxygen vacancy migration energy barrier in the orthorhombic λ phase Ta₂O₅," *Comput. Mater. Sci.* **169**, 109148 (2019).
- ⁴²J. H. Hur, "First principles study of oxygen vacancy activation energy barrier in zirconia-based resistive memory," *Sci. Rep.* **10**, 5405 (2020).
- ⁴³L. Larcher, "Statistical simulation of leakage currents in MOS and flash memory devices with a new multiphonon trap-assisted tunneling model," *IEEE Trans. Electron Devices* **50**, 1246–1253 (2003).
- ⁴⁴Jülich Supercomputing Centre, "JURECA: Data centric and booster modules implementing the modular supercomputing architecture at Jülich supercomputing centre," *J. Large-Scale Res. Facil.* **7**, A182 (2021).